

# Ground State and Finite Temperature Lanczos Methods

P. Prelovšek<sup>1,2</sup> and J. Bonča<sup>1,2</sup>

<sup>1</sup> J. Stefan Institute, SI-1000 Ljubljana, Slovenia

<sup>2</sup> Faculty of Mathematics and Physics, University of Ljubljana, SI-1000 Ljubljana, Slovenia

`peter.prelovsek@ijs.si`, `janez.bonca@ijs.si`

**Abstract.** The present review will focus on recent development of exact-diagonalization (ED) methods that use Lanczos algorithm to transform large sparse matrices onto the tridiagonal form. We begin with a review of basic principles of the Lanczos method for computing ground-state static as well as dynamical properties. Next, generalization to finite-temperatures in the form of well established finite-temperature Lanczos method is described. The latter allows for the evaluation of temperatures  $T > 0$  static and dynamic quantities within various correlated models. Several extensions and modification of the latter method introduced more recently are analysed. In particular, the low-temperature Lanczos method and the micro-canonical Lanczos method, especially applicable within the high- $T$  regime. In order to overcome the problems of exponentially growing Hilbert spaces that prevent ED calculations on larger lattices, different approaches based on Lanczos diagonalization within the reduced basis have been developed. In this context, recently developed method based on ED within a limited functional space is reviewed. Finally, we briefly discuss the real-time evolution of correlated systems far from equilibrium, which can be simulated using the ED and Lanczos-based methods, as well as approaches based on the diagonalization in a reduced basis.

## 1.1 Introduction

Models of strongly correlated systems have been one of the most intensively studied theoretical subjects in the last two decades, stimulated at first by the discovery of compounds superconducting at high-temperatures and ever since by the emergence of various novel materials and phenomena which could be traced back to strongly correlated electrons in these systems. Recently, cold atoms in optical lattice offer a different realization of strongly correlated quantum entities, whereby these systems can be even tuned closer to theoretical models.

One of the most straightforward methods to numerically deal with the lattice (discrete) models of correlated particles, which are inherently many-body

(MB) quantum systems, is exact diagonalization (ED) of small-size systems. In view of the absence of well - controlled analytical methods, ED method has been employed intensively to obtain results for static and dynamical properties of various models with different aims: a) to search and confirm novel phenomena specific for strongly correlated systems, b) to test theoretical ideas and analytical results, c) to get reference results for more advanced numerical techniques.

MB quantum lattice models of interacting particles are characterized with a dimension of the Hilbert space given by the number of basis states  $N_{st} \propto K^N$  that is in turn exponentially increasing with the lattice size  $N$ , where  $K$  is the number of local quantum states. It is therefore clear that ED methods can treat fully only systems with limited  $N_{st}$ , i.e., both  $K$  and  $N$  must be quite modest.

Among the ED approaches the full ED within the Hilbert space of the model Hamiltonian, yielding all eigenenergies and eigenfunctions, is the simplest to understand, most transparent and easy to implement. In principle it allows the evaluation of any ground state (g.s.) property as well as finite temperature  $T > 0$  static or dynamic quantity, at the expense of very restricted  $N_{st}$ . In spite of that, it represents a very instructive approach but also remains essentially the only practical method when all exact levels are needed, e.g., for studies of level statistics.

Lanczos-based ED methods have already long history of applications since Cornelius Lanczos [1] proposed the diagonalization of sparse matrices using the iterative procedure, allowing for much bigger Hilbert spaces  $N_{st}$  relative to full ED. Lanczos diagonalization technique is at present a part of standard numerical linear algebra procedures [2, 3] and as such in solid state physics mainly used to obtain the g.s. energies and wavefunction with corresponding expectation values. The approach has been quite early on extended to calculation of the dynamical response functions within the g.s. [4]. The method has been in the last 20 years extensively used in connection with models related to high- $T_c$  materials, for which we can refer to an earlier overview [5].

The present review will focus on recent development of ED-based and Lanczos-based methods. The basics of the Lanczos method are presented in Sec.1.2 and its application for g.s. properties in Sec.1.3. One of already established generalizations is the finite-temperature Lanczos method (FTLM) [6, 7], reviewed in Sec.1.4, which allows for the evaluation of  $T > 0$  static and dynamic properties within simplest models. Several extensions and modifications of the latter have been introduced more recently, in particular the low-temperature Lanczos method (LTLM) [8] and the microcanonical Lanczos method (MCLM) [9], particularly applicable within the high- $T$  regime.

Since the application of the ED methods there have been attempts and proposals for the proper choice of reduced basis which could allow for the study of bigger systems. While this is clearly very broad subject with most substantial achievements in one-dimensional (1D) systems within the framework of the density-matrix renormalization-group (DMRG) idea, there are

also successful applications in higher  $D > 1$  combined with the Lanczos procedure being reviewed in Sec.1.5. Recently, there is also quite an intensive activity on studies of real-time evolution of correlated systems, both under the equilibrium and the non-equilibrium conditions that can be simulated using the ED and Lanczos-based methods, as discussed in Sec.1.7.

## 1.2 Exact diagonalization and Lanczos method

### 1.2.1 Models, geometries and system sizes

ED-based methods are mostly restricted to simple models with only few local quantum states  $K$  per lattice site in order to reach reasonable system sizes  $N$ . Consequently, there are only few classes of MB models that so far exhaust the majority of ED and Lanczos-method studies, clearly also motivated and influenced by the challenging physics and relevance to novel materials and related experiments.

To get some feeling for available sizes reachable within the ED-based approaches, it should be reminded that in full ED routines the CPU time scales with the number of operations  $Op \propto N_{st}^3$ , while the memory requirement is related to the storage of the whole Hamiltonian matrix and all eigenvectors, i.e.,  $Mem \propto N_{st}^2$ . This limits at present stage of computer facilities the full ED method to  $N_{st} < 2 \cdot 10^4$  MB states. On the other hand, using the Lanczos-based iterative methods for the diagonalization of sparse matrices (Hamiltonians), CPU and memory requirements scale as  $Op, Mem \propto N_{st}$ , at least in their basic application, to calculate the g.s. and its wavefunction. In present-day applications this allows the consideration of much larger basis sets, i.e.,  $N_{st} < 10^9$ . Still, lattice sizes  $N$  reached using the Lanczos technique remain rather modest, compared to some other numerical approaches as the DMRG and quantum-Monte-Carlo (QMC) methods, if the full Hilbert basis space relevant for the model is used.

The simplest nontrivial class of MB lattice models are spin models, the prototype being the anisotropic Heisenberg model for coupled  $S = 1/2$  spins,

$$H = \sum_{\langle ij \rangle \alpha} J_{ij}^{\alpha\alpha} S_i^\alpha S_j^\alpha, \quad (1.1)$$

where the sum  $\langle ij \rangle$  runs over pairs of lattice sites with an arbitrary interaction  $J_{ij}^{\alpha\alpha}$  (being in principle anisotropic) and  $S_i^\alpha$  are component of local  $S = 1/2$  operator. The model has  $K = 2$  quantum states per lattice site and therefore allows for biggest  $N$  in the ED-based approaches where  $N_{st} \propto 2^N$  basis states. To reduce  $N_{st}$  as many symmetries and good quantum numbers as practically possible are used to decompose the Hamiltonian into separate blocks. Evident choice are sectors with the ( $z$ -component of) total spin  $S_{tot}^z$  and the wavevector  $\mathbf{q}$  for systems with periodic boundary conditions, but further also rotational

symmetries of particular lattices have been used. In this way system sizes up to  $N \sim 36$  (for largest and most interesting sector  $S_{tot}^z = 0$ ) have been reached so far using the Lanczos technique without any basis reduction.

On the basis of this simple model one can already discuss the feasibility of the Lanczos-based methods with respect to other numerical quantum MB methods. For the g.s. in 1D spin systems more powerful methods allowing for much bigger systems are DMRG and related approaches. For unfrustrated models in  $D > 1$  the QMC methods are superior for the evaluation of static quantities at any  $T$ . Still, Lanczos-based methods become competitive or at least not superseded for frustrated spin models (where QMC can run into minus-sign problem) or for dynamical properties at  $T > 0$ .

Next in complexity and very intensively studied prototype model is the  $t$ - $J$  model, representing strongly correlated itinerant electrons with an anti-ferromagnetic (AFM) interaction between their spins,

$$H = - \sum_{\langle ij \rangle s} (t_{ij} \tilde{c}_{js}^\dagger \tilde{c}_{is} + \text{H.c.}) + J \sum_{\langle ij \rangle} \mathbf{S}_i \cdot \mathbf{S}_j, \quad (1.2)$$

where due to the strong on-site repulsion doubly occupied sites are forbidden and one is dealing with projected fermion operators  $\tilde{c}_{is} = c_{is}(1 - n_{i,-s})$ . The model can be considered as a good microscopic model for superconducting cuprates which are doped Mott insulators. For a theoretical and experimental overview of Mott insulators and metal-insulator transitions see Ref. [10]. and has been therefore one of the most studied using the Lanczos method [5]. It has  $K = 3$  quantum states per lattice site and besides  $S_{tot}^z$  and  $\mathbf{q}$ , also the number of electrons  $N_e$  (or more appropriate the number of holes  $N_h = N - N_e$ ) are the simplest quantum numbers to implement. Since the model reveals an interesting physics in  $D > 1$ , the effort was in connection with high- $T_c$  cuprates mostly on 2D square lattice. Here the alternative numerical methods have more drawbacks (e.g., minus sign problem in QMC methods due to the itinerant character of fermions) so Lanczos-based methods are still competitive, in particular for getting information on  $T > 0$  dynamics and transport. The largest systems considered with Lanczos method so far are 2D square lattice with  $N = 32$  sites and  $N_h = 4$  holes [11].

Clearly, one of the most investigated within the MB community is the standard single-band Hubbard model, which has  $K = 4$  states per lattice site. Due to the complexity  $N_{st} \propto 4^N$  the application of ED and Lanczos-based method is already quite restricted reaching so far  $N = 20$  sites [12] requiring already  $N_{st} \sim 10^9$  basis states. The model is also the subject of numerous studies using more powerful QMC method and various cluster dynamical-mean-field-theory (DMFT) methods for much larger lattices so Lanczos-based approaches have here more specific goals.

Since reachable lattices for above mentioned models are rather small it is important to choose properly their geometries. This is not the problem in 1D models, but becomes already essential for 2D lattices, analysed in connection

with novel materials, in particular high- $T_c$  cuprates and related materials. In order to keep the periodic boundary conditions for 2D square lattice the choice of Pythagorean lattices with  $N = \lambda_x^2 + \lambda_y^2$  with  $\lambda_x, \lambda_y$  [13] has significantly extended available sizes. Some of frequently used are presented in Fig.1.1. Taking into account only even  $N$  such lattices include  $N = 8, 10, 16, 18, 20, 26, 32, 36$  sites. While unit cells of such lattices are squares, it has been observed that they are not always optimal with respect to the number of next-nearest-neighbors and further nearest neighbors. It has been claimed and partly tested that better results are obtained with slightly deformed lattices (still with periodic boundary conditions) which at the same time offer an even bigger choice of sizes [14].

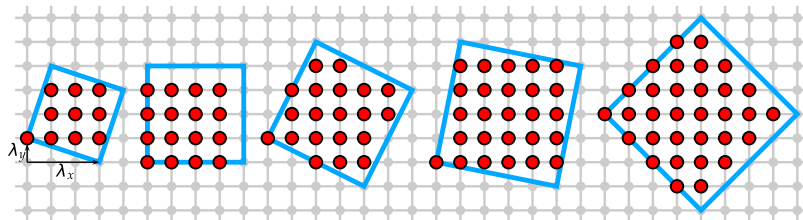


**Fig. 1.1.** Tilted clusters used in 2D square-lattice studies

### 1.2.2 Lanczos diagonalization technique

The Lanczos technique is a general procedure to transform and reduce a symmetric  $N_{st} \times N_{st}$  matrix  $A$  to a symmetric  $M \times M$  tridigonal matrix  $T_M$ . From the chosen initial  $N_{st}$ -dimensional vector  $\mathbf{v}_1$  one generates an orthogonal basis of  $\{\mathbf{v}_1, \dots, \mathbf{v}_M\}$  vectors which span the Krylow space  $\{\mathbf{v}_1, \mathbf{A}\mathbf{v}_1, \dots, \mathbf{A}^{M-1}\mathbf{v}_1\}$  [1–3, 15].

In usual applications for the quantum MB system defined with the Hamiltonian operator  $H$  the Lanczos algorithm starts with a normalized vector  $|\phi_0\rangle$ , chosen as a random vector in the relevant Hilbert space with  $N_{st}$  basis states. The procedure generates orthogonal Lanczos vectors  $L_M = \{|\phi_m\rangle, m = 0, M\}$  spanning the Krylow space  $\{|\phi_0\rangle, H|\phi_0\rangle, \dots, H^M|\phi_0\rangle\}$ . Steps are as follows:  $H$  is applied to  $|\phi_0\rangle$  and the resulting vector is split in components parallel to  $|\phi_0\rangle$ , and normalized  $|\phi_1\rangle$  orthogonal to it, respectively,

$$H|\phi_0\rangle = a_0|\phi_0\rangle + b_1|\phi_1\rangle. \quad (1.3)$$

Since  $H$  is Hermitian,  $a_0 = \langle\phi_0|H|\phi_0\rangle$  is real, while the phase of  $|\phi_1\rangle$  can be chosen so that  $b_1$  is also real. In the next step  $H$  is applied to  $|\phi_1\rangle$ ,

$$H|\phi_1\rangle = b'_1|\phi_0\rangle + a_1|\phi_1\rangle + b_2|\phi_2\rangle, \quad (1.4)$$

where  $|\phi_2\rangle$  is orthogonal to  $|\phi_0\rangle$  and  $|\phi_1\rangle$ . It follows also  $b'_1 = \langle\phi_0|H|\phi_1\rangle = b_1$ . Proceeding with the iteration one gets in  $i$  steps

$$H|\phi_i\rangle = b_i|\phi_{i-1}\rangle + a_i|\phi_i\rangle + b_{i+1}|\phi_{i+1}\rangle, \quad 1 \leq i \leq M. \quad (1.5)$$

where in Eq.(1.5) by construction there are no terms involving  $|\phi_{i-2}\rangle$  etc. By stopping the iteration at  $i = M$  and setting  $b_{M+1} = 0$ , the Hamiltonian can be represented in the basis of orthogonal Lanczos functions  $|\phi_i\rangle$  as the tridiagonal matrix  $H_M$  with diagonal elements  $a_i, i = 0, M$ , and off-diagonal ones  $b_i, i = 1, M$ . Such a matrix is easily diagonalized using standard numerical routines to obtain approximate eigenvalues  $\epsilon_j$  and corresponding orthonormal eigenvectors  $|\psi_j\rangle$ ,

$$|\psi_j\rangle = \sum_{i=0}^M v_{ji}|\phi_i\rangle, \quad j = 0, M. \quad (1.6)$$

It is important to realize that  $|\psi_j\rangle$  are (in general) not exact eigenfunctions of  $H$ , but show a remainder. On the other hand, it is evident from the diagonalization of  $H_M$  that matrix elements

$$\langle\psi_i|H|\psi_j\rangle = \epsilon_j\delta_{ij}, \quad i, j = 0, M, \quad (1.7)$$

are diagonal independently of  $L_M$  (but provided  $i, j \leq M$ ), although the values  $\epsilon_j$  can be only approximate.

If in the equation (1.5)  $b_{M+1} = 0$ , we have found a  $(M + 1)$ -dimensional eigenspace where  $H_M$  is already an exact representation of  $H$ . This inevitably happens when  $M = N_{st} - 1$ , but for  $M < N_{st} - 1$  it can only occur if the starting vector is orthogonal to some invariant subspace of  $H$  which we avoid by choosing the input vector  $|\phi_0\rangle$  as a random one.

It should be recognized that the Lanczos approach is effective only for sparse Hamiltonians, characterized by the connectivity of each basis state with  $K_n \ll N_{st}$  basis states. All prototype discrete tight-binding models discussed in Sec.1.2.1 are indeed of such a type in the local MB basis. Estimating the computation requirements, the number of operations  $Op$  needed to perform  $M$  Lanczos iterations scales as  $Op \propto K_n M N_{st}$ . The main restriction is still in memory requirements due to large  $N_{st}$ . A straightforward application of Eq.(1.5) would require the fast storage of all  $|\phi_i\rangle, i = 0, M$ , i.e., also the memory capacity  $Mem \propto M N_{st}$ . However, for the evaluation of the eigenvalues alone during the iteration, Eq.(1.5), only three  $|\phi_i\rangle$  are successively required, so this leads to  $Mem \propto 3N_{st}$ . If the Hamiltonian matrix is not evaluated on the fly (simultaneously), then also  $Mem \propto K_n N_{st}$  for the nonzero Hamiltonian matrix elements is needed.

The Lanczos diagonalization is in essence an iterative power method which is known to converge fast for the extreme lower and upper eigenvalues [2,3], clearly in physical application most relevant is the search for the g.s. energy  $E_0$  and corresponding wavefunction  $|\Psi_0\rangle$ . Typically,  $M > 50$  are enough to reach

very high accuracy for both. It is evident that for such modest  $M \ll N_{st}$  one cannot expect any reliable results for eigenstates beyond the few at the bottom and the top of the spectrum. On the other hand, the Lanczos procedure is subject to roundoff errors, introduced by the finite-precision arithmetics which usually only becomes severe at larger  $M > 100$  after the convergence of extreme eigenvalues and is seen as the loss of the orthogonality of vectors  $|\phi_i\rangle$ . It can be remedied by successive reorthogonalization [2, 3, 15] of new states  $|\phi'_i\rangle$ , plagued with errors, with respect to previous ones. However this procedure requires  $Op \sim M^2 N_{st}$  operations, and can become computationally more demanding than Lanczos iterations themselves. This effect also prevents one to use the Lanczos method, e.g., to efficiently tridiagonalize full large matrices [3].

### 1.3 Ground State Properties and Dynamics

After  $|\Psi_0\rangle$  is obtained, the g.s. static properties can be evaluated in principle for any operator  $A$  as

$$\bar{A}_0 = \langle \Psi_0 | A | \Psi_0 \rangle. \quad (1.8)$$

Clearly, the procedure (1.8) for large basis is effective only if operator  $A$  is in the same basis also sparse, as it is in most cases of interest.

It is, however, the advantage of the Lanczos procedure that also g.s. dynamical functions can be calculated within the same framework [4]. Let us consider the dynamical (autocorrelation) response function

$$C(\omega) = \langle \Psi_0 | A^\dagger \frac{1}{\omega^+ + E_0 - H} A | \Psi_0 \rangle, \quad (1.9)$$

for the observable given by the operator  $A$  where  $\omega^+ = \omega + i\epsilon$ ,  $\epsilon > 0$ . To calculate  $C(\omega)$  one has to run the second Lanczos procedure with a new initial function  $|\tilde{\phi}_0\rangle$ ,

$$|\tilde{\phi}_0\rangle = \frac{1}{\alpha} A | \Psi_0 \rangle, \quad \alpha = \sqrt{\langle \Psi_0 | A^\dagger A | \Psi_0 \rangle}. \quad (1.10)$$

Starting with  $|\tilde{\phi}_0\rangle$  one generates another Lanczos subspace  $\tilde{L}_{\tilde{M}} = \{|\tilde{\phi}_j\rangle, j = 0, \tilde{M}\}$  with (approximate) eigenvectors  $|\tilde{\psi}_j\rangle$  and eigenenergies  $\tilde{\epsilon}_j$ . The matrix for  $H$  in the new basis is again a tridiagonal one with  $\tilde{a}_j$  and  $\tilde{b}_j$  elements, respectively. Terminating the Lanczos procedure at given  $\tilde{M}$ , one can evaluate Eq.(1.9) as a resolvent of the  $H_{\tilde{M}}$  matrix expressed in the continued-fraction form [4, 5, 16],

$$C(\omega) = \frac{\alpha^2}{\omega^+ + E_0 - \tilde{a}_0 - \frac{\tilde{b}_1^2}{\omega^+ + E_0 - \tilde{a}_1 - \frac{\tilde{b}_2^2}{\omega^+ + E_0 - \tilde{a}_2 - \dots}}}, \quad (1.11)$$

terminating with  $\tilde{b}_{\tilde{M}+1} = 0$ , although other termination functions can also be employed and well justified.

We note that frequency moments of the spectral function

$$\begin{aligned}\mu_l &= -\frac{1}{\pi} \int_{-\infty}^{\infty} \omega^l \text{Im}C(\omega) d\omega = \langle \Psi_0 | A^\dagger (H - E_0)^l A | \Psi_0 \rangle = \\ &= \alpha^2 \langle \tilde{\phi}_0 | (H - E_0)^l | \tilde{\phi}_0 \rangle,\end{aligned}\quad (1.12)$$

are exact for given  $|\Psi_0\rangle$  provided  $l \leq \tilde{M}$ , since the operator  $H^l, l < \tilde{M}$ , is exactly reproduced within the Lanczos (or corresponding Krylow) space  $\tilde{L}_{\tilde{M}}$ .

Finally,  $C(\omega)$  (1.11) can be presented as a sum of  $j = 0, \tilde{M}$  poles at  $\omega = \tilde{\epsilon}_j - E_0$  with corresponding weights  $w_j$ . As a practical matter we note that in analogy to Eq.(1.6)

$$w_j = |\langle \tilde{\psi}_j | A | \Psi_0 \rangle|^2 = \alpha^2 |\langle \tilde{\psi}_j | \tilde{\phi}_0 \rangle|^2 = \alpha^2 \tilde{v}_{j0}^2, \quad (1.13)$$

hence no matrix elements need to be evaluated within this approach. In contrast to the autocorrelation function (1.11), the procedure allows also the treatment of general correlation functions  $C_{AB}(\omega)$ , with  $B \neq A^\dagger$ . In this case matrix elements  $\langle \Psi_0 | B | \tilde{\psi}_j \rangle$  have to be evaluated explicitly. It should be also mentioned that at least lowest poles of  $C(\omega)$ , Eq.(1.11), should coincide with eigenenergies  $\omega = E_i - E_0$  if  $|\tilde{\phi}_0\rangle$  is not orthogonal to  $|\Psi_0\rangle$ . However, using  $\tilde{M} > 50$  spurious poles can emerge (if no reorthogonalization is used) which, however, carry no weight as also evident from exact moments (1.12).

In this chapter we do not intend to present an overview of applications of the full ED and Lanczos-type studies of g.s. static and dynamical properties of correlated systems. Such investigations have been numerous even before the high- $T_c$  era but intensified strongly with studies of prototype models relevant for high- $T$  cuprates [5] and other novel materials with correlated electrons. Although variety of models have been investigated they are still quite restricted in the number of local degrees and sizes.

## 1.4 Static Properties and Dynamics at $T > 0$

Before describing the Finite temperature Lanczos method (FTLM) we should note that the Lanczos basis is very useful and natural basis to evaluate the matrix elements of the type

$$W_{kl} = \langle n | H^k B H^l A | n \rangle, \quad (1.14)$$

where  $|n\rangle$  is an arbitrary normalized vector, and  $A, B$  are general operators. One can calculate this expression exactly by performing two Lanczos procedures with  $M = \max(k, l)$  steps. The first one, starting with the vector  $|\phi_0\rangle = |n\rangle$ , produces the Lanczos basis  $L_M$  along with approximate eigenstates



$|\psi_j\rangle$  and  $\epsilon_j$ . The second Lanczos procedure is started with the normalized vector  $|\tilde{\phi}_0\rangle \propto A|\phi_0\rangle = A|n\rangle$ , Eq.(1.10), and generates  $\tilde{L}_M$  with corresponding  $|\tilde{\psi}_j\rangle$  and  $\tilde{\epsilon}_j$ . We can now define projectors onto limited subspaces

$$P_M = \sum_{i=0}^M |\psi_i\rangle\langle\psi_i|, \quad \tilde{P}_M = \sum_{i=0}^M |\tilde{\psi}_i\rangle\langle\tilde{\psi}_i|. \quad (1.15)$$

Provided that  $(l, k) < M$  projectors  $P_M$  and  $\tilde{P}_M$  span the whole relevant basis for the operators  $H^k$  and  $H^l$ , respectively, so that one can rewrite  $W_{kl}$  in Eq.(1.14) as

$$W_{kl} = \langle\phi_0|P_M H P_M H \dots H P_M B \tilde{P}_M H \dots \tilde{P}_M H \tilde{P}_M A|\phi_0\rangle. \quad (1.16)$$

Since  $H$  is diagonal in the basis  $|\psi_j\rangle$  and  $|\tilde{\psi}_j\rangle$ , respectively, one can write finally

$$W_{kl} = \sum_{i=0}^M \sum_{j=0}^M \langle\phi_0|\psi_i\rangle\langle\psi_i|B|\tilde{\psi}_j\rangle\langle\tilde{\psi}_j|A|\phi_0\rangle(\epsilon_i)^k(\tilde{\epsilon}_j)^l. \quad (1.17)$$

It is important to note that matrix element expression (1.17) is exact, independent of how (in)accurate representation  $|\psi_i\rangle, \epsilon_i$  and  $|\tilde{\psi}_j\rangle, \epsilon_j$ , respectively, are to true system eigenvalues. The only condition remains that number of Lanczos steps is sufficient, i.e.,  $M > (l, k)$ .

#### 1.4.1 Finite temperature Lanczos method: Static quantities

A straightforward calculation of canonical thermodynamic average of an operator  $A$  at  $T > 0$  (in a finite system) requires the knowledge of all eigenstates  $|\Psi_n\rangle$  and corresponding energies  $E_n$ , obtained, e.g., by the full ED of  $H$ ,

$$\langle A \rangle = \frac{\sum_{n=1}^{N_{st}} e^{-\beta E_n} \langle \Psi_n | A | \Psi_n \rangle}{\sum_{n=1}^{N_{st}} e^{-\beta E_n}}, \quad (1.18)$$

where  $\beta = 1/k_B T$ . Such direct evaluation is both CPU time and storage demanding for larger systems and is at present accessible only for  $N_{st} \sim 10000$ .

In a general orthonormal basis  $|n\rangle$  for finite system with  $N_{st}$  basis states one can express the canonical expectation value  $\langle A \rangle$  as

$$\langle A \rangle = \frac{\sum_{n=1}^{N_{st}} \langle n | e^{-\beta H} A | n \rangle}{\sum_{n=1}^{N_{st}} \langle n | e^{-\beta H} | n \rangle}, \quad (1.19)$$

The FTLM for  $T > 0$  is based on the evaluation of the expectation value in Eq.(1.19) for each starting  $|n\rangle$  using the Lanczos basis. We note that such procedure guarantees correct high- $T$  expansion series (for given finite system) to high order. Let us perform the high- $T$  expansion of Eq.(1.19),

$$\begin{aligned}\langle A \rangle &= Z^{-1} \sum_{n=1}^{N_{st}} \sum_{k=0}^{\infty} \frac{(-\beta)^k}{k!} \langle n | H^k A | n \rangle, \\ Z &= \sum_{n=1}^{N_{st}} \sum_{k=0}^{\infty} \frac{(-\beta)^k}{k!} \langle n | H^k | n \rangle.\end{aligned}\quad (1.20)$$

Terms in the expansion  $\langle n | H^k A | n \rangle$  can be calculated exactly using the Lanczos procedure with  $M \geq k$  steps (with  $|\phi_0^n\rangle = |n\rangle$  as the starting function) since this is a special case of the expression (1.14). Using relation (1.17) with  $l = 0$  and  $B = 1$ , we get

$$\langle n | H^k A | n \rangle = \sum_{i=0}^M \langle n | \psi_i^n \rangle \langle \psi_i^n | A | n \rangle (\epsilon_i^n)^k. \quad (1.21)$$

Working in a restricted basis  $k \leq M$ , we can insert the expression (1.21) into sums (1.20), extending them to  $k > M$ . The final result can be expressed as

$$\begin{aligned}\langle A \rangle &= Z^{-1} \sum_{n=1}^{N_{st}} \sum_{i=0}^M e^{-\beta \epsilon_i^n} \langle n | \psi_i^n \rangle \langle \psi_i^n | A | n \rangle, \\ Z &= \sum_{n=1}^{N_{st}} \sum_{i=0}^M e^{-\beta \epsilon_i^n} \langle n | \psi_i^n \rangle \langle \psi_i^n | n \rangle,\end{aligned}\quad (1.22)$$

and the error of the approximation is  $O(\beta^{M+1})$ .

Evidently, within a finite system Eq.(1.22), expanded as a series in  $\beta$ , reproduces exactly the high- $T$  series to the order  $M$ . In addition, in contrast to the usual high- $T$  expansion, Eq.(1.22) remains accurate also for  $T \rightarrow 0$ . Let us assume for simplicity that the g.s.  $|\Psi_0\rangle$  is nondegenerate. For initial states  $|n\rangle$  not orthogonal to  $|\Psi_0\rangle$ , already at modest  $M \sim 50$  the lowest eigenstate  $|\psi_0^n\rangle$  converges to  $|\Psi_0\rangle$ . We thus have for  $\beta \rightarrow \infty$ ,

$$\langle A \rangle = \frac{\sum_{n=1}^{N_{st}} \langle n | \Psi_0 \rangle \langle \Psi_0 | A | n \rangle}{\sum_{n=1}^{N_{st}} \langle n | \Psi_0 \rangle \langle \Psi_0 | n \rangle} = \langle \Psi_0 | A | \Psi_0 \rangle / \langle \Psi_0 | \Psi_0 \rangle, \quad (1.23)$$

where we have taken into account the completeness of the set  $|n\rangle$ . Obtained result is just the usual g.s. expectation value of an operator.

The computation of static quantities (1.22) still involves the summation over the complete set of  $N_{st}$  states  $|n\rangle$ , which is clearly not feasible in practice. To obtain a useful method, a further essential approximation replaces the full summation over  $|n\rangle$  by a partial one over a much smaller set of random states [17, 18]. Such an approximation is analogous to Monte Carlo methods and leads to a statistical error which can be well estimated and is generally quite small. Let us first consider only the expectation value (1.19) with respect to a single random state  $|r\rangle$ , which is a linear combination of basis states

$$|r\rangle = \sum_{n=1}^{N_{st}} \eta_{rn} |n\rangle, \quad (1.24)$$

where  $\eta_{rn}$  are assumed to be distributed randomly. Then the random quantity can be expressed as

$$\begin{aligned} \tilde{A}_r &= \langle r | e^{-\beta H} A | r \rangle / \langle r | e^{-\beta H} | r \rangle = \\ &= \sum_{n,m=1}^{N_{st}} \eta_{rn}^* \eta_{rm} \langle n | e^{-\beta H} A | m \rangle / \sum_{n,m=1}^{N_{st}} \eta_{rn}^* \eta_{rm} \langle n | e^{-\beta H} | m \rangle. \end{aligned} \quad (1.25)$$

Assuming that due to the random sign (phase) offdiagonal terms with  $\eta_{rn}^* \eta_{rm}$ ,  $m \neq n$  on average cancel for large  $N_{st}$ , we remain with

$$\bar{A}_r = \sum_{n=1}^{N_{st}} |\eta_{rn}|^2 \langle n | e^{-\beta H} A | n \rangle / \sum_{n=1}^{N_{st}} |\eta_{rn}|^2 \langle n | e^{-\beta H} | n \rangle. \quad (1.26)$$

We can express  $|\eta_{rn}|^2 = 1/N_{st} + \delta_{rn}$ . Random deviations  $\delta_{rn}$  should not be correlated with matrix elements  $\langle n | e^{-\beta H} | n \rangle = Z_n$  and  $\langle n | e^{-\beta H} A | n \rangle = Z_n A_n$ , therefore  $\bar{A}_r$  is close to  $\langle A \rangle$  with an statistical error related to the effective number of terms  $\bar{Z}$  in the thermodynamic sum, i.e.

$$\bar{A}_r = \langle A \rangle (1 + \mathcal{O}(1/\sqrt{\bar{Z}})), \quad (1.27)$$

$$\bar{Z} = e^{\beta E_0} \sum_n Z_n = \sum_{n=1}^{N_{st}} \langle n | e^{-\beta(H-E_0)} | n \rangle. \quad (1.28)$$

Note that for  $T \rightarrow \infty$  we have  $\bar{Z} \rightarrow N_{st}$  and therefore at large  $N_{st}$  very accurate average (1.28) can be obtained even from a single random state [17,18]. On the other hand, at finite  $T < \infty$  the statistical error of  $\bar{A}_r$  increases with decreasing  $\bar{Z}$ .

To reduce statistical error, in particular at modest  $T > 0$ , within the FTLM we sum in addition over  $R$  different randomly chosen  $|r\rangle$ , so that in the final application Eq.(1.22) leads to

$$\begin{aligned} \langle A \rangle &= \frac{N_{st}}{\bar{Z}R} \sum_{r=1}^R \sum_{j=0}^M e^{-\beta \epsilon_j^r} \langle r | \psi_j^r \rangle \langle \psi_j^r | A | r \rangle, \\ Z &= \frac{N_{st}}{R} \sum_{r=1}^R \sum_{j=0}^M e^{-\beta \epsilon_j^r} |\langle r | \psi_j^r \rangle|^2. \end{aligned} \quad (1.29)$$

Random states  $|r\rangle = |\phi_0^r\rangle$  serve as initial functions for the Lanczos iteration, resulting in  $M$  eigenvalues  $\epsilon_j^r$  with corresponding  $|\psi_j^r\rangle$ . The relative statistical error is reduced by sampling (both for  $\langle A \rangle$  and  $Z$ ) and behaves as

$$\delta \langle A \rangle / \langle A \rangle = \mathcal{O}(1/\sqrt{R\bar{Z}}). \quad (1.30)$$

For general operator  $A$  the calculation of  $|\psi_j^r\rangle$  and corresponding matrix elements  $\langle\psi_j^r|A|r\rangle$  is needed. On the other hand, the calculation effort is significantly reduced if  $A$  is conserved quantity, i.e.,  $[H, A] = 0$ , and can be diagonalized simultaneously with  $H$ . Then

$$\langle A \rangle = \frac{N_{st}}{ZR} \sum_{r=1}^R \sum_{j=0}^M e^{-\beta\epsilon_j^r} |\langle r|\psi_j^r\rangle|^2 A_j^r. \quad (1.31)$$

In this case the evaluation of eigenfunctions is not necessary since the element  $\langle r|\psi_j^r\rangle = v_{j0}^r$ , Eq.(1.6), is obtained directly from eigenvectors of the tridiagonal matrix  $H_M^r$ . There are several quantities of interest which can be evaluated in this way, in particular the thermodynamic properties as internal energy, specific heat, entropy, as well as uniform susceptibility etc. [7, 19].

Taking into account all mentioned assumptions, the approximation  $\langle A \rangle$  (1.29) yields a good estimate of the thermodynamic average at all  $T$ . For low  $T$  the error is expected to be of the order of  $\mathcal{O}(1/\sqrt{R})$ , while for high  $T$  the error is expected to scale even as  $\mathcal{O}(1/\sqrt{N_{st}R})$ . Since arguments leading to these estimates are not always easy to verify, it is essential to test the method for particular cases.

#### 1.4.2 Finite temperature Lanczos method: Dynamical response

The essential advantage of the FTLM with respect to other methods is nevertheless in the calculation of dynamical quantities. Let us consider the dynamical susceptibility as given by the autocorrelation function  $C(\omega)$  (procedure for the general correlation function  $C_{AB}(\omega)$  is given in Ref. [7]),

$$\chi''(\omega) = \pi(1 - e^{-\beta\omega})C(\omega), \quad C(\omega) = \frac{1}{\pi} \text{Re} \int_0^{+\infty} dt e^{i\omega t} C(t), \quad (1.32)$$

with

$$C(t) = \langle A^\dagger(t)A(0) \rangle = \frac{1}{Z} \sum_n \langle n|e^{(-\beta+it)H} A^\dagger e^{-iHt} A|n\rangle. \quad (1.33)$$

Expanding the exponentials in analogy to static quantities, Eq.(1.20), we get

$$C(t) = Z^{-1} \sum_{n=1}^{N_{st}} \sum_{k,l=0}^{\infty} \frac{(-\beta+it)^k}{k!} \frac{(-it)^l}{l!} \langle n|H^k A^\dagger H^l A|n\rangle. \quad (1.34)$$

Expansion coefficients in Eq.(1.34) can be again obtained via the Lanczos method, as discussed in Sec.1.4.1. Performing two Lanczos iterations with  $M$  steps, started with normalized  $|\phi_0^n\rangle = |n\rangle$  and  $|\tilde{\phi}_0^n\rangle \propto A|n\rangle$ , respectively, we calculate coefficients  $W_{kl}$  following the equation (1.17). We again note that (within the full basis  $|n\rangle$ ) the series are via  $W_{kl}$  exactly evaluated within the

Lanczos basis up to order  $l, k \leq M$ . The latter yields through Eq.(1.34) a combination of  $(\beta, t)$  expansion, i.e. a combination of high- $T$ , short- $t$  (in frequency high- $\omega$ ) expansion to very high order. Extending and resumming series in  $k$  and  $l$  into exponentials, we get in analogy with Eq.(1.20)

$$C(t) = Z^{-1} \sum_{n=1}^{N_{st}} \sum_{i,j=0}^M e^{-\beta \epsilon_i^n} e^{it(\epsilon_i^n - \tilde{\epsilon}_j^n)} \langle n | \psi_i^n \rangle \langle \psi_i^n | A^\dagger | \tilde{\psi}_j^n \rangle \langle \tilde{\psi}_j^n | A | n \rangle, \quad (1.35)$$

Finally replacing the full summation with the random sampling the FTLM recipe for the correlation function is

$$C(\omega) = \frac{N_{st}}{ZR} \sum_{r=1}^R \sum_{i,j=1}^M e^{-\beta \epsilon_i^r} \langle r | \psi_i^r \rangle \langle \psi_i^r | A^\dagger | \tilde{\psi}_j^r \rangle \langle \tilde{\psi}_j^r | r \rangle \delta(\omega - \tilde{\epsilon}_j^r + \epsilon_i^r). \quad (1.36)$$

We check the nontrivial  $T = 0$  limit of above expression. If  $|n\rangle$  are not orthogonal to the g.s.  $|\Psi_0\rangle$ , then for large enough  $M$  the lowest-lying state converges to  $\epsilon_0^n \sim E_0$  and  $|\psi_0^n\rangle \sim |\Psi_0\rangle$ , respectively. In this case we have

$$C(\omega, T = 0) \approx \frac{N_{st}}{R} \sum_{r=1}^R \sum_{j=0}^M \langle \Psi_0 | A^\dagger | \tilde{\psi}_j^r \rangle \langle \tilde{\psi}_j^r | A | r \rangle \langle r | \Psi_0 \rangle \delta(\omega + E_0 - \tilde{\epsilon}_j^r) \quad (1.37)$$

At  $T \sim 0$  one needs in general  $M \gg 100$  in order that at least low-lying states relevant to Eq.(1.37) approach  $|\tilde{\psi}_j^r\rangle \rightarrow |\Psi_j\rangle$  and  $\tilde{\epsilon}_j^r \rightarrow E_j$ . Also a considerable sampling  $R > 1$  is required to get correct also amplitudes of separate peaks in the spectrum of Eq.(1.37) which are a subject of a statistical error due to the incomplete projection on different random  $|r\rangle$  in  $\langle \tilde{\psi}_j^r | A | r \rangle \langle r | \Psi_0 \rangle$ . Similar statistical error can in fact appear also for static quantities in Eq.(1.29).

### 1.4.3 Finite temperature Lanczos method: Implementation

Most straightforward is the implementation of the FTLM for static quantities, Eq.(1.29). In particular for conserved quantities, Eq.(1.31), the computation load is essentially that of the g.s. Lanczos iteration repeated  $R$  times and only a minor changes are needed within the usual g.s. Lanczos code.

On the other hand, for the dynamical correlation function (1.36) the memory requirement as well as the CPU time is dominated mostly by the evaluation of the matrix element  $\langle \psi_i^r | A^\dagger | \tilde{\psi}_j^r \rangle$  where the operations scale as  $Op \propto RM^2 N_{st}$  and memory as  $Mem \propto MN_{st}$ . This effectively limits the application of the FTLM to  $50 < M < 500$  where the lower bound is determined by the convergence of the g.s.  $|\Psi_0\rangle$ . Still, it should be noted that the calculation can be done simultaneously (without any additional cost) for all desired  $T$ , since matrix elements are evaluated only once. Evidently, one should use as much as possible symmetries of the Hamiltonian, e.g.,  $N_e, S_{tot}^z, \mathbf{q}$  to reduce effective  $N_{st}$  by splitting the sampling over different symmetry sectors.

The effect of finite  $M$  is less evident. Since  $M \sim 100$  is enough to converge well few lowest levels, it is also generally satisfactory for reliable dynamical correlation functions at low  $T$ . At high  $T$ , however, one can observe very regular oscillations which are the artifact of the Lanczos iterations with  $M \ll N_{st}$ . Namely, the procedure generates between extreme eigenvalues quite equidistant spectrum of quasi-states with the level spacing  $\Delta\epsilon \sim \Delta E/M$ , where  $\Delta E$  is the full energy span of MB eigenstates. The effect is well visible in Fig.1.2 where the high- $T$  result for the spin structure factor  $S(q = \pi, \omega)$  for the 1D Heisenberg model, Eq.(1.1), is presented for various  $M$ . It is evident that for the presented case ( $N = 24$  and  $\Delta E \sim 16J$ )  $M > 200$  is sufficient to obtain smooth spectra even for high  $T \gg J$ . However, larger  $M$  are advisable if sharper structures persist at high  $T$ .

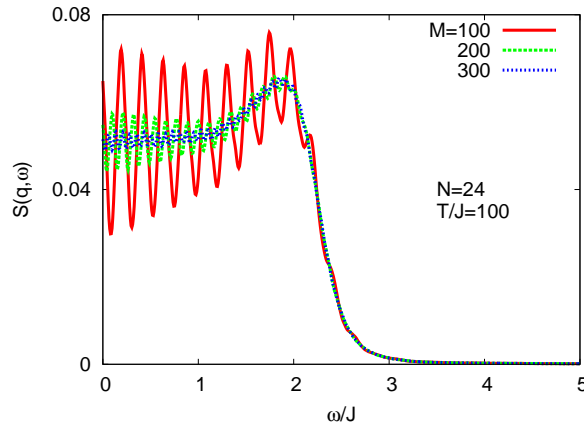


**Fig. 1.2.** High- $T$  spin structure factor  $S(q = \pi, \omega)$  for the 1D Heisenberg model, as calculated with different number of Lanczos steps  $M$ .

The role of random sampling  $R$  is less important for intermediate and high  $T$  since the relative error is largely determined via  $\bar{Z}$  as evident from Eq.(1.28). Larger  $R \gg 1$  is necessary only for the correct limit  $T \rightarrow 0$  (for given system size) and for off-diagonal operators  $A$ .

One can claim that the FTLM in general obtains for all reachable systems results which are at any  $T$  very close to exact (full ED) results for the same finite (given  $N$ ) system and the accuracy can be improved by increasing  $M$  and  $R$ . Still, it remains nontrivial but crucial to understand and have in control finite size effects.

At  $T = 0$  both static and dynamical quantities are calculated from the g.s.  $|\Psi_0\rangle$ , which can be quite dependent on the size and on the shape of the system. At least in 1D for static quantities the finite-size scaling  $N \rightarrow \infty$  can be performed in a controlled way, although in this case more powerful methods as, e.g., the DMRG are mostly available. In higher dimensional lattices,

e.g., in 2D systems finite-size scaling is practically impossible due to very restricted choice of small sizes and different shapes. Also g.s. ( $T = 0$ ) dynamical quantities are often dominated by few (typically  $N_p < M$ ) peaks which are finite-size dominated [5]. On the other hand,  $T > 0$  generally introduces the thermodynamic averaging over a large number of eigenstates. This directly reduces finite-size effects for static quantities, whereas for dynamical quantities spectra become denser. From Eq.(1.36) it follows that we get in spectra at elevated  $T > 0$  typically  $N_p \propto RM^2$  different peaks resulting in nearly continuous spectra. This is also evident from the example of a high- $T$  result in Fig.1.2.

It is plausible that finite-size effects at  $T > 0$  become weaker. However, it should be recognized that there could exist several characteristic length scales in the considered physical (and model) system, e.g. the antiferromagnetic (AFM) correlation length  $\xi$ , the transport mean free path  $l_s$  etc. These lengths generally decrease with increasing  $T$  and results for related quantities get a macroscopic relevance provided that  $\xi(T), l_s(T) < L$  where  $L \propto N^{1/d}$  is the linear size of the system. However, there exist also anomalous cases, e.g., in an integrable system  $l_s$  can remain infinite even at  $T \rightarrow \infty$  [20,21].

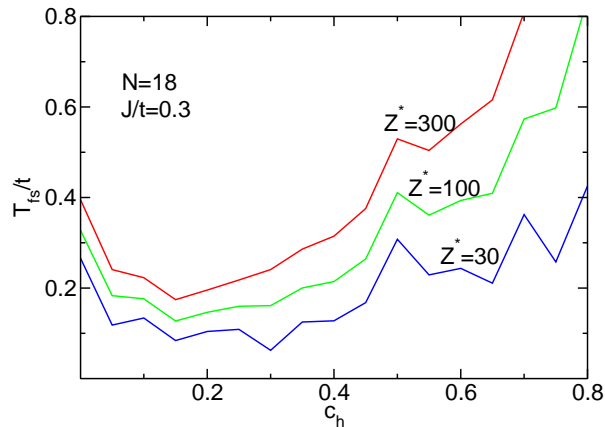


**Fig. 1.3.** Finite-size temperature  $T_{fs}$  vs. hole doping  $c_h$  in the 2D  $t$ - $J$  model with  $J/t = 0.3$ , as calculated with the FTLM in system of  $N = 18$  sites [7].

A simple criterion for finite size effects one can use the normalized thermodynamic sum  $\bar{Z}(T)$ , Eq.(1.28), which provides the effective number of MB states contributing at chosen  $T$  (note that for a system with a nondegenerate g.s.  $\bar{Z}(T = 0) = 1$ ). Finite-size temperature  $T_{fs}$  can be thus defined with the relation  $\bar{Z}(T_{fs}) = Z^*$  where in practice the range  $10 < Z^* < 50$  is reasonable.

Clearly, the FTLM is best suited just for systems with a large density of low lying MB states, i.e., for large  $\bar{Z}$  at low  $T$ .

Since  $\bar{Z}(T)$  is directly related to the entropy density  $s$  and the specific heat  $C_v$  of the system, large  $\bar{Z}$  at low  $T$  is the signature of frustrated quantum MB systems which are generally difficult to cope with other methods (e.g., the QMC method). Such are typically examples of strongly correlated electrons with an inherent frustration, e.g., the doped AFM and the  $t$ - $J$  model, Eq.(1.2), in the strong correlation regime  $J < t$ . We present in Fig.1.3 as an example the variation of  $T_{fs}$  in the 2D  $t$ - $J$  model with the hole doping  $c_h = N_h/N$ , as calculated for different  $Z^* = 30 - 300$  for the fixed system of  $N = 18$  sites and  $J/t = 0.3$  as relevant for high- $T$  cuprates. It is indicative that  $T_{fs}$  reaches the minimum for intermediate (optimum) doping  $c_h = c_h^* \sim 0.15$ , where we are able to reach  $T_{fs}/t \sim 0.1$ . Away from the optimum doping  $T_{fs}$  is larger, i.e., low-energy spectra are quite sparse both for undoped AFM and even more for effectively noninteracting electrons far away from half-filling (for nearly empty or full band).

#### 1.4.4 Low Temperature Lanczos Method

The standard FTLM suffers at  $T \rightarrow 0$  from a statistical error due to finite sampling  $R$ , both for the static quantities, Eqs.(1.29),(1.30), as well as for the dynamical correlations, Eqs.(1.36),(1.37). The discrepancy can be easily monitored by the direct comparison with the g.s. Lanczos method, Eqs.(1.8,1.11). To avoid this problem, a variation of the FTLM method, named Low-temperature Lanczos method (LTLM) has been proposed [8] which obtains correct g.s. result (for finite systems) independent of the sampling  $R$ .

The idea of LTLM is to rewrite Eq.(1.19) in a symmetric form

$$\langle A \rangle = \frac{1}{Z} \sum_{n=1}^{N_{st}} \langle n | e^{-\beta H/2} A e^{-\beta H/2} | n \rangle, \quad (1.38)$$

and insert the Lanczos basis in analogy with the FTLM, Eq.(1.19), now represented with a double sum

$$\langle A \rangle = \frac{N_{st}}{ZR} \sum_{r=1}^R \sum_{j,l=0}^M e^{-\beta(\epsilon_j^r + \epsilon_l^r)/2} \langle r | \psi_j^r \rangle \langle \psi_j^r | A | \psi_l^r \rangle \langle \psi_l^r | r \rangle, \quad (1.39)$$

The advantage of the latter form is that it satisfies the correct  $T = 0$  limit provided that the g.s. is well converged, i.e.,  $|\psi_0^r\rangle \sim |\Psi_0\rangle$ . It then follows from Eq.(1.39),

$$\langle A \rangle = \sum_{r=1}^R \langle r | \Psi_0 \rangle \langle \Psi_0 | A | \Psi_0 \rangle \langle \Psi_0 | r \rangle / \sum_{r=1}^R \langle \Psi_0 | r \rangle \langle r | \Psi_0 \rangle = \langle \Psi_0 | A | \Psi_0 \rangle, \quad (1.40)$$

for any chosen set of  $|r\rangle$ . For the dynamical correlations  $C(t)$  one can in straightforward way derive the corresponding expression in the Lanczos basis



$$\begin{aligned}
 C(\omega) &= \frac{N_{st}}{ZR} \sum_{r=1}^R \sum_{i,j,l=0}^M e^{-\beta(\epsilon_i^r + \epsilon_l^r)/2} \langle r | \psi_i^r \rangle \langle \psi_i^r | A^\dagger | \tilde{\psi}_j^{r,l} \rangle \langle \tilde{\psi}_j^{r,l} | A | \psi_l^r \rangle \langle \psi_l^r | r \rangle \times \\
 &\times \delta(\omega - \tilde{\epsilon}_j^{r,l} + \frac{1}{2}(\epsilon_i^r + \epsilon_l^r)).
 \end{aligned} \tag{1.41}$$

It is again evident that for  $T \rightarrow 0$  the sampling does not influence results being correct even for  $R = 1$  if the g.s.  $|\Psi_0\rangle$  is well converged for all starting  $|r\rangle$ . The payoff is in an additional summation over the new Lanczos basis which starts from each  $A|\psi_l^r\rangle$  in Eq.(1.40). Since the LTLM is designed for lower  $T$  there one can effectively restrict summations in  $(i, l)$  in Eq.(1.41) to much smaller  $M' \ll M$  where only lowest states with  $\epsilon_i^r, \epsilon_l^r \sim E_0$  contribute [8], and in addition use smaller  $M_1 \ll M$  for the basis  $|\tilde{\psi}_j^{r,l}\rangle$ .

An alternative version for Lanczos-type approach [22] for dynamical quantities is not to start the second Lanczos run from  $A|r\rangle$  [7] or from  $A|\psi_l^r\rangle$  [8], but from

$$|\tilde{A}r\rangle = \sum_{l=0}^M A|\psi_l^r\rangle e^{-\beta\epsilon_l^r/2} \langle \psi_l^r | r \rangle. \tag{1.42}$$

In this way one obtains with the second Lanczos run the Lanczos eigenstates  $|\tilde{\psi}_k^r\rangle$ , which cover the relevant Hilbert space for starting random vector  $|r\rangle$  and the inverse temperature  $\beta$ . The resulting dynamical autocorrelation function is

$$\begin{aligned}
 C(\omega) &= \frac{N_{st}}{RZ} \sum_{r=1}^R \sum_{i,k=0}^M e^{-\beta\epsilon_i^r/2} \langle r | \psi_i^r \rangle \langle \psi_i^r | A^\dagger | \tilde{\psi}_j^r \rangle \langle \tilde{\psi}_j^r | \tilde{A}r \rangle \times \\
 &\times \delta(\omega - \tilde{\epsilon}_j^r + \epsilon_i^r).
 \end{aligned} \tag{1.43}$$

In this way the sufficiency of only one random vector in the  $T = 0$  limit is reproduced, while at  $T > 0$  the algorithm has the same time efficiency as the FTLM, but with much smaller random sampling needed to reach the same accuracy (at least for low  $T$ ). However, the price paid is that results for each  $T$  need to be calculated separately, while within the FTLM all  $T$  (or  $T$  up to certain value within the LTLM) are evaluated simultaneously.

#### 1.4.5 Microcanonical Lanczos Method

While most investigations in strongly correlated systems focus on the low- $T$  regime, there are systems where dynamical properties are nontrivial even at high  $T$ . Well known such case is the spin diffusion constant  $D_s(T)$  in the isotropic Heisenberg model, Eq.(1.1), which is not known by value and moreover not even its existence at any  $T > 0$ . Similar although somewhat less controversial is the case of transport quantities, both for integrable or generic nonintegrable models. Whereas the FTLM seems well adapted for studies of transport response functions, oscillations due to limited  $M$  can affect the crucial low- $\omega$  resolution as seen also in Fig.1.2.

At elevated  $T$  it is therefore an advantage to use the Microcanonical Lanczos method (MCLM) [9], employing the fact from statistical physics that in the thermodynamic limit (for large system) the microcanonical ensemble should yield the same results as the canonical one. The shortcoming of the MCLM emerges since in finite systems statistical fluctuations are much larger within the microcanonical ensemble. Still, reachable finite-size systems have very high density of states in the core of the MB spectrum as probed by high  $T$ . Hence, statistical fluctuations are at high  $T$  effectively smoothed out in contrast to low- $T$  properties dominated by a small number of low lying MB states.

The implementation of the MCLM is quite simple and straightforward. One first determines the target energy  $\lambda = \langle H \rangle(T)$  which represents the microcanonical energy equivalent to the canonical average energy for chosen  $T$  and the system size  $N$ . Since  $\lambda$  is a parameter within the MCLM, one can relate it to  $T$  by performing either FTLM (simplified due to conserved quantity  $H$ ) on the same system or extrapolating full ED results (with linear dependence on  $N$ ) on small lattices. Next we find a representative microcanonical state  $|\Psi_\lambda\rangle$  for the energy  $\lambda$ . One convenient way within the Lanczos-type approach is to use the new operator

$$V = (H - \lambda)^2. \quad (1.44)$$

Performing Lanczos iterations with the operator  $V$  yields again the extremum eigenvalues, in particular the lowest one close to  $V \sim 0$ . In contrast to the g.s. procedure, the convergence to a true eigenstate cannot be reached in system sizes of interest even with  $M_1 \gg 100$ . The reason is extremely small eigenvalue spacing of operator  $V$  scaling as  $\Delta V_n \propto (\Delta E/N_{st})^2$ ,  $\Delta E$  being the whole energy span within the given system. Fortunately such a convergence is not necessary (even not desired) since the essential parameter is small energy uncertainty  $\sigma_E$ , given by

$$\sigma_E^2 = \langle \Psi_\lambda | V | \Psi_\lambda \rangle. \quad (1.45)$$

For small energy spread  $\sigma_E/\Delta E < 10^{-3}$  typically  $M_1 \sim 1000$  is needed. Again, to avoid storing  $M_1$  Lanczos wavefunctions  $|\phi_i\rangle$  Lanczos procedure is performed twice as described in Sec.1.2.2, i.e., the second time with known tridiagonal matrix elements to calculate finally  $|\Psi_\lambda\rangle$  in analogy with Eq.(1.6). The latter is then used to evaluate any static expectation average  $\langle A \rangle$  or the dynamical correlation function as in Eq.(1.9),

$$C(\omega, \lambda) = \langle \Psi_\lambda | A^\dagger \frac{1}{\omega^+ + \lambda - H} A | \Psi_\lambda \rangle. \quad (1.46)$$

The latter is evaluated again using Lanczos iterations with  $M_2$  steps starting with the initial wavefunction  $|\tilde{\phi}_0\rangle \propto A|\Psi_\lambda\rangle$  and  $C(\omega)$  is represented in terms of continued fractions. Since the MB levels are very dense and correlation functions smooth at  $T \gg 0$  large  $M_2 \gg 100$  are needed but as well easily reachable to achieve high- $\omega$  resolution in  $C(\omega)$ .

It is evident that the computer requirement for the MCLM both regarding the CPU and memory are essentially the same as for the g.s. dynamical calculations except that typically  $M_1, M_2 \gg 100$ . In particular requirements are less demanding than using the FTLM with  $M > 100$ . A general experience is that for systems with large  $N_{st} \gg 10000$  the MCLM dynamical results agree very well with FTLM results for the same system. It should be also noted that actual frequency resolution  $\delta\omega$  in  $C(\omega)$ , Eq.(1.46), is limited by  $\delta\omega \sim \sigma_E$  which is, however, straightforward to improve by increasing  $M_1, M_2$  with typical values  $M_1, M_2 > 1000$ . One can also improve MCLM results for any  $T$  by performing an additional sampling over initial random starting  $|\phi_0\rangle$  as well as over  $\lambda$  with a probability distribution  $p(\lambda)$  simulating the canonical ensemble in a finite-size system, i.e., by replacing Eq.(1.46) with

$$C(\omega) = \sum_{\lambda} p(\lambda) C(\omega, \lambda). \quad (1.47)$$

#### 1.4.6 Statical and dynamical quantities at $T > 0$ : Applications

The FTLM has been designed to deal with simplest tight-binding models of strongly correlated electrons, at the time mostly with challenging microscopic electronic models of high- $T_c$  superconductors [6, 7], where besides superconductivity there is a variety of anomalous non-Fermi-like properties even in the normal state. Clearly of interest in this connection are prototype MB models as the Heisenberg model, Eq.(1.1), the  $t$ - $J$  model, Eq.(1.2) and the Hubbard model on the 2D square lattice. Unfrustrated Heisenberg model can be numerically studied on much bigger lattices with QMC and related methods. The 2D Hubbard model was and still is mostly subject of DMFT and QMC studies, since at half-filling or close to it the Lanczos methods are quite restricted due to large  $N_{st}$  even for modest sizes  $N \sim 16$ . Therefore one focus of Lanczos-based approaches was on the  $t$ - $J$  model being with some generalizations a microscopic representation of electronic properties of high- $T_c$  cuprates.

Thermodynamic quantities as chemical potential  $\mu$ , entropy density  $s$ , specific heat  $C_v$  are the easiest to implement within the FTLM. Their  $T$ - and (hole) doping  $c_h$ -dependence within the  $t$ - $J$  model on a 2D square lattice (calculated up to  $N = 26$  sites) reveal already very anomalous behavior of doped Mott insulators [23] (as evident already from Fig.1.3), confirmed also by results for more complete Hubbard model [24]. An introduction of next-neighbor hopping  $t'$  generates also an asymmetry in thermodynamic properties between hole-doped and electron-doped cuprates [25] as well quite dramatic influence of stripe order [26] consistent with the physics of cuprates.

The advantages of the FTLM and also its feasibility for the 2D  $t$ - $J$  model are even more evident in quite numerous studies of spin and charge dynamics at  $T > 0$  [7] which show good agreement with neutron scattering and NMR [19,27–29], optical conductivity  $\sigma(\omega)$  and resistivity  $\rho(T)$  [30,31], Hall constant  $R_H(T)$  [32] and a general non-Fermi-liquid behavior of cuprates [29], as well as

the puzzling strong influence of nonmagnetic impurities [33]. As an example of a transport quantity hardly accessible by other methods we present in Fig.1.4 the universal planar resistivity  $\rho(T)$ , as extracted from the dynamical conductivity  $\sigma(\omega \rightarrow 0) = 1/\rho$ , within the  $t$ - $J$  model for different doping levels  $c_h$  [31]. Result in Fig.1.4 clearly shows a linear dependence below the pseudogap temperature  $T^*$  dependent on doping  $c_h$ . Another characteristic signature is a saturation (plateau) of  $\rho(T)$  at low doping and the universal trend at high  $T$ .

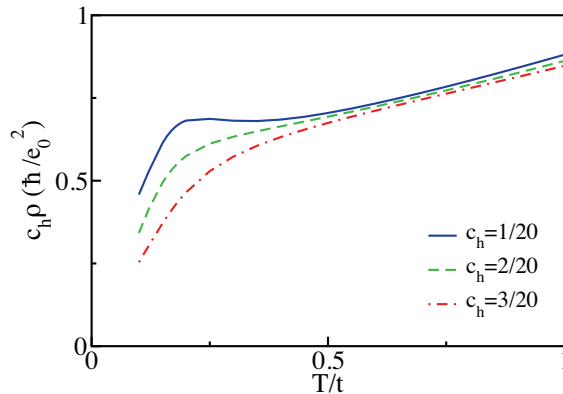


**Fig. 1.4.** Normalized 2D resistivity  $c_h \rho$  vs.  $T/t$  within the  $t$ - $J$  model with  $J/t = 0.3$  for different hole concentrations  $c_h$  [31].

Spectral properties as manifested in single-particle spectral functions  $A(\mathbf{k}, \omega)$  are in the core of the understanding of cuprates, as well as of strongly correlated electrons in general. Here, even g.s. and low- $T$  properties are the challenge for numerical studies whereby the FTLM can be viewed as a controlled way to get reliable (macroscopic-like)  $T \rightarrow 0$  result, in contrast to quite finite-size plagued results obtained via g.s. Lanczos procedure [5]. Using the FTLM at  $T \sim T_{fs}$  with the twisted boundary condition can simulate a continuous wavevector  $\mathbf{k}$ . Using in addition the course graining averaging one can reach results for  $A(\mathbf{k}, \omega)$  [34–36] giving insight into the electron vs. hole doped angle-resolved photoemission experiments, quasiparticle relaxation and waterfall-like effects. A characteristic result of such studies is in Fig.1.5 for the single-particle density of states  $\mathcal{N}(\omega) = \sum_{\mathbf{k}} A(\mathbf{k}, \omega)$  [34]. Here, the strength of the FTLM is visible in the high  $\omega$  resolution within the most interesting low- $\omega$  window. Interesting and reproducible are also nontrivial spectral shapes as the sharp peak close to  $\omega < 0$  and a broad shoulder for  $\omega \ll 0$ . Most im-

portant is, however, the evident pseudogap (observed also experimentally in cuprates) visible at  $\omega \sim 0$  in the low-doping regime.

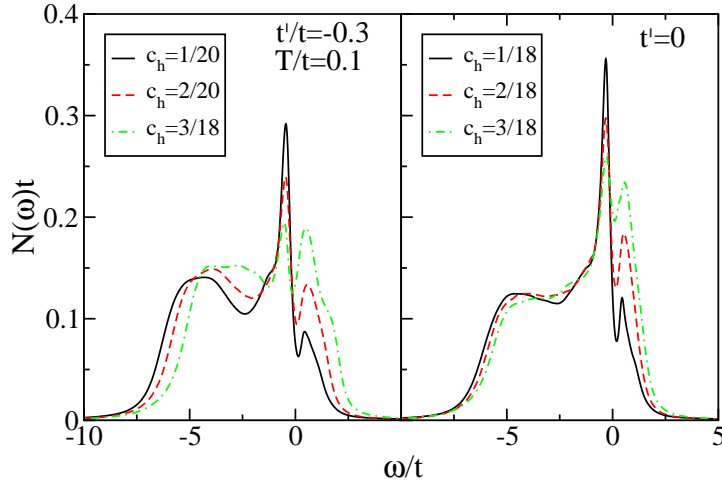


**Fig. 1.5.** Density of states  $\mathcal{N}(\omega)$  for different dopings  $c_h$  within the extended  $t$ - $J$  model with n.n.n. hopping  $t' = -0.3t$  and  $t' = 0$ , respectively [34].

Besides the challenging models for cuprates there have been also studies of static and dynamical properties of multiband and multiorbital models which either reduce to the generalized  $t$ - $J$  model [37] or to Kondo lattice models [38–40] and the Falicov-Kimball model [41]. While the increasing number of local basis states  $K$  clearly limits the applicability of ED-based methods, they are competitive in treating nontrivial frustrated spin models less suitable for the QMC and other methods, however closely related to physics of novel materials. Moreover, frustrated models are characterized by a large entropy density  $s$  and related low  $T_{fs}$  essential conditions for feasibility of FTLM results. Examples of such systems are the Shastry-Sutherland model [42, 43], 2D  $J_1$ - $J_2$  model [44], and properties of frustrated magnetic molecules [45–47].

Another class of problems which can be quite effectively dealt with the FTLM and MCLM approaches is the fundamental as well as experimentally relevant problem of transport in 1D systems of interacting fermions as realized, e.g., in quasi-1D spin-chain materials [48]. It has been recognized that the transport response at any  $T > 0$  crucially differs between integrable and nonintegrable systems. Since the 1D isotropic as well as anisotropic Heisenberg model, Eq.(1.1), is integrable it opens a variety of fundamental questions of anomalous transport in such systems, the effects of perturbative terms and impurities. Such fundamental questions on transport and low- $\omega$  dynamic response remain nontrivial even at high  $T$  [20, 21], hence the MCLM is the most feasible and straightforward method. It has been in fact first probed on

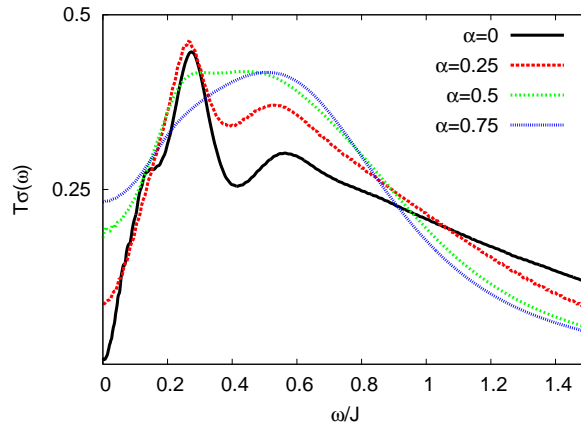


**Fig. 1.6.** High- $T$  dynamical spin conductivity  $T\sigma(\omega)$  within the anisotropic Heisenberg model in the Ising-like regime  $\Delta = 1.5$  and various next-neighbor interaction  $\alpha = J_2^z/J$  as calculated with the MCLM on a chain with  $N = 30$  sites.

the anomalous transport in 1D insulators [49] but further used to study interaction-induced transport at  $T > 0$  in disordered 1D systems [50, 51], incoherent transport induced by a single either static [52] or dynamical spin impurity [53].

In Fig.1.6 we present as an example the MCLM result for the dynamical spin conductivity in the anisotropic Heisenberg model, Eq.(1.1), where  $J^{zz} \neq J^{xx} = J^{yy} = J$  in the Ising-like (with the spin gap in the g.s.) regime  $\Delta = J^{zz}/J > 1$ . Results for the high- $T$  dynamical spin conductivity  $T\sigma(\omega)$  are shown for various next-neighbor (anisotropic) coupling  $\alpha = J_2^z/J$ . First message is that the MCLM as the method is well adapted for the high- $\omega$  resolution (here using  $M_1 = M_2 = 2000$ ) and reaching large  $N = 30$  ( $N_{st} \sim 5.10^6$  in a single  $S^z = 0, q$  sector). Another conclusion is that the dynamics of such systems is very anomalous. For the integrable case  $\alpha = 0$  we find  $\sigma_0 = \sigma(0) \sim 0$  but also an anomalous finite-size peak at  $\omega_p \propto 1/N$  [49]. At the same time breaking integrability with  $\alpha > 0$  appears to lead to  $\sigma_0 > 0$  still approaching an 'ideal' insulator (insulating at all  $T$ ) for a weak perturbation  $\sigma_0(\alpha \rightarrow 0) \rightarrow 0$  [54].

## 1.5 Reduced Basis Lanczos Methods

The main shortcoming of ED approaches are finite-size effects that tamper calculations on small lattice systems. Exponentially growing Hilbert spaces represent the main obstacle against extending ED calculations to larger lattices. One way to extend ED calculations is to reduce the complete Hilbert space and keep only states that give a significant weight in the g.s. wavefunc-

tion or in the relevant Hilbert space, e.g., at  $T > 0$ . Here, the crucial step represents developing a feasible algorithm for the basis reduction.

One clear example of very effective basis construction is the DMRG method, most feasible for 1D correlated systems. Within this method, described in other chapters, some intermediate steps of ED diagonalization are frequently also performed via Lanczos iterations [55]. Moreover, there are recently developments which are extending the application of DMRG procedure to  $T > 0$  dynamical response [56, 57] involving more directly features of Lanczos-based approaches. In particular, recent finite- $T$  dynamical DMRG (FTD-DMRG) method [57] combines the DMRG selection of MB states and the LTLM procedure as described in Sec.1.4.3 and in Eqs.(1.42), (1.43) to evaluate dynamical correlations at  $T > 0$ , both being effective at low  $T$ . So far the FTD-DMRG method has been applied to find novel features within the 1D  $J_1$ - $J_2$  model [58].

The ideas to find the reduced basis sets is, however, more general going beyond the 1D systems and has been successful in solving several problems of strongly correlated systems. Even before the discovery of high- $T_c$  superconductors that boosted research on models of correlated systems, Brinkman and Rice [59] developed a string representation of configurational space to compute the band renormalization and mobility in the atomic limit of the Hubbard model. The string picture was later used to compute single hole properties and to estimate hole-pair binding within the  $t$ - $J$  model by many authors [60]. In connection with ED calculations on finite lattices the truncation scheme based on the limitation of the maximal length of strings leads to slow convergence in terms of the number of reduced basis states [61] in the spin-isotropic limit of the  $t$ - $J$  model. Rather slow convergence is achieved also using a cluster diagonalization scheme together with the systematic expansion of the Hilbert space [62].

The exact diagonalization method in limited functional space (EDLFS) was originally developed specifically for solving the problem of a single charge carrier (hole) doped in the AFM background [63]. The basic principle of the method is based on the above mentioned string picture, that emerges as a moving hole through the AFM background creates in its wake paths of overturned spins - strings. EDLFS was later generalized to include phonon degrees of freedom [64, 65]. For the purpose of presenting the method we start by considering the prototype  $t$ - $J$  model, Eq.(1.2), coupled to dispersionless optical phonons on a square lattice

$$\begin{aligned}
 H &= H_t + H_J + H_g + H_{\omega_0} = \\
 &= -t \sum_{\langle ij \rangle_s} \tilde{c}_{i_s}^\dagger \tilde{c}_{j_s} + J \sum_{\langle ij \rangle} \left[ S_i^z S_j^z + \frac{\gamma}{2} (S_i^+ S_j^- + S_i^- S_j^+) \right] + \\
 &+ g \sum_i (1 - n_i) (a_i^+ + a_i) + \omega_0 \sum_i a_i^+ a_i, \tag{1.48}
 \end{aligned}$$





relative to the Néel state (spin flips), and occupation numbers representing excited phonon quanta,

$$|\phi\rangle = |\mathbf{r}_h; \mathbf{r}_1, \mathbf{r}_2, \dots, \mathbf{r}_{N_{fl}}; n_{\mathbf{r}'_1}, n_{\mathbf{r}'_2}, \dots, n_{\mathbf{r}'_{N_s}}\rangle, \quad (1.50)$$

where  $\mathbf{r}_i$  represent spin-flip coordinates,  $n_{\mathbf{r}'_j}$  number of phonon quanta at site  $\mathbf{r}'_j$  and  $N_{fl} \leq N_s$  is the total number of spin flips.

Since the Hilbert space grows exponentially with  $N_s$  there exist many intuitive physically motivated restrictions optimizing LFS's for different parameter regimes to slow down the exponential growth. A systematic control over the growing Hilbert space can be achieved through realization that the diagonal energy of long strings grows linearly with  $N_s$ . Assuming that the contribution of long strings in the g.s. wave-function is negligible, we introduce an additional parameter  $N_b \leq N_s$  that restricts generation of long strings by imposing a condition under which all coordinates of spin flips satisfy  $|\mu_h - \mu_f| \leq N_b; \mu = \{x, y\}$  where  $h$  and  $f$  refer to hole and spin-flip indexes, respectively. Application of this condition improves the quality of the LFS by increasing the number of states containing spin flips in the vicinity of the hole while keeping the total amount of states within computationally accessible limits.

Fig.1.7 represents a particular state generated using Eq.(1.49). Black and grey dots represent sites with spins 'up' and 'down', respectively. The hole starts at the position  $(-1, 1)$  in the direction  $(0, -1)$ , and travels along the path indicated by arrows. Crosses represent spin-flips and numbers represent excited phonon quanta, generated along the hole's path. The effect of the parameter  $m$  is to set the maximal number of excited phonon quanta on indicated positions. In this particular parent the hole ends its path on the B-sublattice. Using allowed minimal translations, the position of the hole in the parent state is at  $\mathbf{r}_h = (1, 0)$ .

After the generation of LFS the full Hamiltonian in Eq.(1.48) is diagonalized within this LFS using the standard Lanczos procedure. The efficiency of the EDLFS method in case of the  $t - J$  model and stability of results against varying  $N_s$  and  $N_b$  has been shown in detail in Ref. [63].

Besides reliable results obtained using the EDLFS there are other important advantages over most other methods: a) it is highly efficient, b) the method is free of finite-size effects, c) it treats spin and lattice degrees of freedom on the same footing while preserving the full quantum nature of the problem, and d) it allows for computation of physical properties at an arbitrary wavevector. Even though results depend on the choice of parameters defining the functional generator in Eq.(1.49), such as  $N_s$  and  $m$ , reliable results are obtained already for relatively small sizes of the Hilbert space  $N_{st}$ , typically up to three orders of magnitude smaller than in the case of exact diagonalization techniques. For most static as well as dynamic quantities convergence to the thermodynamic limit can be achieved with a systematic increase of  $N_s$  and  $m$ .

The EDLFS obviously has few limitations: a) the method is limited to calculations in the zero-doping limit, e.g.,  $N_h = 1, 2$  mobile particles immersed in an infinite (AFM) background, b) the spin anisotropy is inherently built in the method, and c) due to the broken translational symmetry of the starting wavefunction, calculations are limited to the reduced AFM Brillouin zone.

Due to its high efficiency in dealing with spin fluctuation the method represents one of the few successful methods that allows the addition of lattice degrees of freedom to a correlated electron model. The EDLFS handles spin and lattice degrees of freedom by preserving the full quantum mechanical nature of the problem and enables a direct calculation of the dynamic response functions in terms of real frequency  $\omega$ .

The EDLFS can be rather in a straightforward way generalized for the study of the two-hole  $N_h = 2$  problem [66, 67]. ED studies in the  $t$ - $J$  model for  $N_h = 2$  were performed on a 2D square lattices up to  $N = 32$  sites [68]. Still, the maximal distance between two holes remains rather small  $l_{\max} = \sqrt{N/2} = 4$ . Attempts to increase the lattices sizes beyond ED studies led authors to investigate various truncated basis approaches [61, 62] and using small sets of variational wavefunctions with given rotational symmetries based on 'string' and 'spin - bag' pictures [69].

While the problem of two holes within the  $t$ - $J$  model represents a challenging problem, the addition of quantum phonons seems an almost unachievable task. Nevertheless, the EDLFS due to an efficient choice of LFS can handle this problem well. The construction of the LFS starts from a Néel state with holes located on neighboring sites and with zero phonon quanta. Such a state represents a parent state of a translationally invariant state. We generate new parent states in analogy with Eq.(1.49) by applying the generator of states

$$\{|\phi_l\rangle_a\} = \left( H_t + \tilde{H}_J + \sum_{i=1}^m H_g^i \right)^{n_s} |\phi_0\rangle_a \quad (1.51)$$

where  $\tilde{H}_J$  denotes the off-diagonal spin exchange term in Eq.(1.48) applied only to erase spin flips generated through application of  $H_t$ . This allows the creation of states with holes positioned further apart that are not connected with spin strings. Note that for larger  $N_s \geq 6$  some of such states would be generated even without evoking  $\tilde{H}_J$  term via the Trugman loops [60]. One of the advantages of this method in comparison to other approaches is that it allows much larger distances between the holes,  $l_{\max} = N_s + 1$ . Note also that the functional generator preserves as well the point-group symmetry.

As an example we present in Fig.1.8 the probability of finding a hole pair at a distance  $r$

$$P(r) = \left\langle \sum_{\langle i \neq j \rangle} n_i^h n_j^h \delta(|\mathbf{r}_i - \mathbf{r}_j| - r) \right\rangle, \quad (1.52)$$

where  $n_i^h = 1 - n_i$  is local hole density. In the case of dimensionless electron-phonon coupling  $\lambda = g^2/8\omega_0 t = 0$ , the maximal allowed distance between

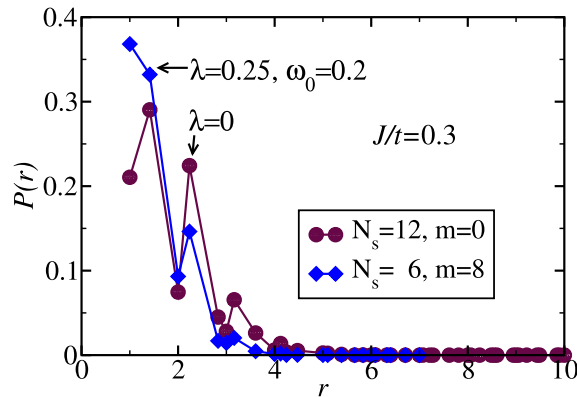


**Fig. 1.8.** Probability  $P(r)$  of finding a hole pair at a distance  $r$  within the  $t$ - $J$ -Holstein model with  $J/t = 0.3$  and  $\omega_0/t = 0.2$ , evaluated for electron-phonon coupling parameters  $\lambda = 0$  and  $\lambda = 0.25$ . Different  $N_s$  and  $m$  as indicated in legends were chosen giving  $N_{st} \sim 7.10^6$  and  $N_{st} \sim 26.10^6$ , respectively. Both solutions correspond to a  $d$ -wave symmetry.

holes is  $l_{\max} = 13$  while for  $\lambda = 0.25$   $l_{\max} = 7$ , whereby results for  $\lambda = 0$  are consistent with previous findings using ED [68], reduced-basis ED [62], as well as string picture variational approaches [69].

## 1.6 Real Time Dynamics using Lanczos Method

Research in the field of non-equilibrium dynamics of complex quantum systems constitutes a formidable theoretical challenge. When dealing with ED approaches or calculations in the reduced basis, the time evolution of the time - dependent Schrödinger equation,

$$i \frac{\partial \Psi(t)}{\partial t} = H(t) \Psi(t), \quad (1.53)$$

can be efficiently obtained using the time - dependent Lanczos technique, as originally described in Ref. [70] and later applied and analysed in more detail [71]. One of the straightforward reasons is that most commonly the Lanczos method is used to compute g.s. of MB Hamiltonian. Generalizing the method to time - dependent calculation represents only a minor change to already existing codes. Even though the method is most suitable for the time evolution of the time - independent Hamiltonian, it can nevertheless be applied even to the time - dependent case. The time evolution of  $|\Psi(t)\rangle$  is then calculated by step-wise change of time  $t$  in small time increments  $\delta t$ ,

generating at each step Lanczos basis of dimension  $M$  (typically  $M < 10$ ), to follow the evolution

$$|\Psi(t + \delta t)\rangle \simeq e^{-iH(t)\delta t}|\Psi(t)\rangle \simeq \sum_{l=1}^M e^{-i\epsilon_l\delta t}|\psi_l\rangle\langle\psi_l|\Psi(t)\rangle, \quad (1.54)$$

where  $|\psi_l\rangle, \epsilon_l, l = 0, M$  are Lanczos eigenfunctions and eigenvalues, respectively, obtained via the Lanczos iteration started with  $|\phi_0\rangle = |\Psi(t)\rangle$ . The advantage of the time-evolution method following Eq.(1.54) is that it preserves the normalization of  $|\Psi(t + \delta t)\rangle$  for arbitrary large  $\delta t$ . The approximation of finite  $M$  in Eq.(1.54) is also correct at least to the  $M$ -th Taylor-expansion order in  $\delta t$ . It is, however, important to stress that  $\delta t$  should be chosen small enough to take into account properly the time-dependence of  $H(t)$ . E.g., in the case of driving the system with an external constant electric field,  $\delta t/t_B \sim 10^{-3}$  where  $t_B$  is the Bloch oscillation period [54, 72–74].

So far, investigations of correlated driven systems under the influence of a driving electric field in 1D systems using the Lanczos time evolution method focused on generic systems, like the metallic and Mott - insulating regime within the 1D model of interacting spinless fermions [54, 72]. Even though rather small systems can be studied it has been established that steady state can be reached without any additional coupling to a heat bath, provided that the Joule heating of the system is properly taken into account.

The case of a single charge carrier in an inelastic medium driven by the external electric field in 1D as well as 2D has been investigated using EDLFS combined with a Lanczos-based time-evolution approach [72, 74, 75]. The strength of EDLFS is in construction of the Hilbert space that enables not only an accurate description of the ground state of the single carrier system but it allows for enough extra inelastic (spin or phonon) excitations to absorb energy, emitted by the field driven carrier, until the system reaches the steady state. This again enables a proper description of the steady state without coupling the system to an external thermal bath.

## 1.7 Discussion

Exact diagonalization based methods, both the full ED and Lanczos-type ED approach, are very extensively employed in the investigations of strongly correlated MB quantum systems in solid state and elsewhere. The reason for their widespread use are several: a) unbiased approach to the MB problem without any simplifications or approximations, independent of complexity of the MB system, b) relative simplicity of generating the codes for various models and observables, c) easy and straightforward testing of codes, d) direct interpretation of obtained quantum MB states and their possible anomalous structure and properties, e) high pedagogical impact as a quick and at the same time very nontrivial introduction into the nature of MB quantum physics.

Also the Lanczos-based methods described in this review, i.e., the g.s. Lanczos method for static and dynamic quantities, and somewhat more elaborate FTLM, MCLM, LTLM and EDLFS, require rather modest programming efforts in comparison with more complex numerical methods, e.g., the QMC- and DMRG- based methods, as described in other chapters.

Clearly, the main drawback of ED methods is the smallness of lattice sizes  $N$  determined by a limited number of basis states (at present  $N_{st} < 10^9$ ) treated with a Lanczos iteration procedure. The achievable  $N$  with ED methods appears quite modest in comparison with some established and recently developed numerical methods, as the QMC, DMRG, matrix-product-states methods etc. Still, in spite of very intensive development and advance of novel numerical methods in last two decades there are several aspects of strong-correlation physics, where ED-based methods are so far either the only feasible or at least superior to other methods. In this chapter we have focused mostly on Lanczos-based methods and applications where they are still competitive and get nontrivial results with a macroscopic validity:

- a) MB g.s. and its properties of frustrated and complex models mostly so far do not offer alternative powerful methods except ED approaches, at least beyond  $D = 1$  systems where DMRG-based methods can be effectively applied,
- b)  $T > 0$  static properties evaluated with Lanczos-based methods as the FTLM and the LTLM are as well most powerful and reliable for frustrated and complex system, in particular in systems with high degeneracies of MB states and large entropy at low  $T$ ,
- c)  $T > 0$  Lanczos methods for dynamical quantities, as the FTLM and MCLM, yield for many models and geometries results superior to other methods or even the only accessible results in several cases. In particular the advantage of the latter methods is high  $\omega$  resolution at all temperatures beyond the finite size limit  $T > T_{fs}$ , the macroscopic-like results at low  $T$  with a proper scaling to  $T \rightarrow 0$ , and the possibility of detailed studies of systems with nontrivial (anomalous) dynamics at any, in particular high  $T$ .
- d) Lanczos technique of ED is also the natural application within the methods with a restricted MB basis sets as the EDLFS and DMRG-type targeting as well as in the real-time evolution studies of strongly correlated systems.

## References

1. C. Lanczos, J. Res. Nat. Bur. Stand., **45**, 255 (1950).
2. B. N. Parlett, *The Symmetric Eigenvalue Problem* (Prentice Hall, Eaglewood Cliffs) (1980).
3. J. W. Demmel, *Applied Numerical Linear Algebra*, (SIAM, Philadelphia) (1997).
4. R. Haydock, V. Heine, and M. J. Kelly, J. Phys. C: Solid State Phys. **8**, 2591 (1975).
5. for a review, see E. Dagotto, Rev. Mod. Phys. **66**, 763 (1994).
6. J. Jaklič and P. Prelovšek, Phys. Rev. B **49**, 5065 (1994).
7. for a review, see J. Jaklič and P. Prelovšek, Adv. Phys. **49**, 1 (2000).

8. M. Aichhorn, M. Daghofer, H. G. Evertz, and W. von der Linden, *Phys. Rev. B* **67**, 161103(R) (2003).
9. M. W. Long, P. Prelovšek, S. El Shawish, J. Karadamoglou, and X. Zotos, *Phys. Rev. B* **68**, 235106 (2003).
10. for a review, see M. Imada, A. Fujimori, and Y. Tokura, *Rev. Mod. Phys.* **70**, 1039 (1998).
11. P.W. Leung, *Phys. Rev. B* **73**, 14502 (2006).
12. T. Tohyama, Y. Inoue, K. Tsutsui, and S. Maekawa, *Phys. Rev. B* **72**, 045113 (2005).
13. J. Oitmaa and D. D. Betts, *Can. J. Phys.* **56**, 897 (1978).
14. D. D. Betts, H. Q. Lin, and J. S. Flynn, *Can. J. Phys.* **77**, 3535 (1999); P. R. C. Kent, M. Jarrell, T. A. Maier, and Th. Pruschke, *Phys. Rev. B* **72**, 060411 (2005)
15. J. Cullum and R. A. Willoughby, *J. Comp. Phys.* **44**, 329 (1981).
16. H. Mori, *Prog. Theor. Phys.* **34**, 423 (1965).
17. M. Imada and M. Takahashi, *J. Phys. Soc. Jpn.* **55**, 3354 (1986).
18. R. N. Silver and H. Röder, *Int. J. Mod. Phys. C* **5**, 735 (1995).
19. J. Jaklič and P. Prelovšek, *Phys. Rev. Lett.* **75**, 1340 (1995).
20. X. Zotos and P. Prelovšek, *Phys. Rev. B* **53**, 983 (1996).
21. for a review, see F. Heidrich - Meisner, A. Honecker, and W. Brenig, *Eur. Phys. J. Special Topics* **151**, 135 (2007).
22. J. Kokalj, Ph.D. Thesis, unpublished.
23. J. Jaklič and P. Prelovšek, *Phys. Rev. Lett.* **77**, 892 (1996).
24. J. Bonča and P. Prelovšek, *Phys. Rev. B* **67**, 180502(R) (2003).
25. T. Tohyama and S. Maekawa, *Phys. Rev. B* **67**, 092509 (2003).
26. T. Tohyama, S. Maekawa, and P. Prelovšek, *Phys. Rev. B* **67**, 180502 (2003).
27. Y. Shibata, T. Tohyama, and S. Maekawa, *Phys. Rev. B* **64**, 054519 (2001).
28. P. Prelovšek, I. Sega, and J. Bonča, *Phys. Rev. Lett.* **92**, 027002 (2004).
29. J. Bonča, P. Prelovšek, and I. Sega, *Phys. Rev. B* **70**, 224505 (2004).
30. J. Jaklič and P. Prelovšek, *Phys. Rev. B* **50**, 7129 (1994).
31. M. M. Zemljich and P. Prelovšek, *Phys. Rev. B* **72**, 075108 (2005).
32. D. Veberič and P. Prelovšek, *Phys. Rev. B* **66**, 020408(R) (2002).
33. P. Prelovšek and I. Sega, *Phys. Rev. Lett.* **93**, 207202 (2004).
34. M. M. Zemljich and P. Prelovšek, *Phys. Rev. B* **75**, 104514 (2007).
35. M. M. Zemljich, P. Prelovšek, and T. Tohyama, *Phys. Rev. B* **76**, 012502 (2007).
36. M. M. Zemljich, P. Prelovšek, and T. Tohyama, *Phys. Rev. Lett.* **100**, 036402 (2008).
37. P. Horsch, J. Jaklič and F. Mack, *Phys. Rev. B* **59**, 6217 (1999).
38. K. Haule, J. Bonča, and P. Prelovšek, *Phys. Rev. B* **61**, 2482 (2000)
39. P. Horsch, J. Jaklič and F. Mack, *Phys. Rev. B* **59**, 14149(R) (1999).
40. I. Zerec, B. Schmidt, and P. Thalmeier, *Phys. Rev. B* **73**, 245108 (2006).
41. S. El Shawish, J. Bonča, and D. Batista, *Phys. Rev. B* **68**, 195112 (2003).
42. S. El Shawish, J. Bonča, and I. Sega, *Phys. Rev. B* **72**, 184409 (2005).
43. S. El Shawish, A. Ramšak, and J. Bonča, *Phys. Rev. B* **75**, 205442 (2007).
44. B. Schmidt, P. Thalmeier, and N. Shannon, *Phys. Rev. B* **76**, 125113 (2007).
45. J. Schnack and O. Wendland, *Eur. Phys. J. B* **78**, 535 (2010).
46. J. Schnack, arXiv:1012.4980.
47. M. Haertel, J. Richter, D. Ihle, J. Schnack, and S.-L. Drechsler, arXiv:1106.1013.
48. for a review, see C. Hess, *Eur. Phys. J. Special Topics* **151**, 73 (2007).

49. P. Prelovšek, S. El Shawish, X. Zotos, and M. Long, *Phys. Rev. B* **70**, 205129 (2004).
50. A. Karahalios, A. Metavitsiadis, X. Zotos, A. Gorczyca, and P. Prelovšek, *Phys. Rev. B* **79**, 024425 (2009).
51. O. S. Barišić and P. Prelovšek, *Phys. Rev. B* **82**, 161106 (2010).
52. O. S. Barišić, P. Prelovšek, A. Metavitsiadis, and X. Zotos, *Phys. Rev. B* **80**, 125118 (2009).
53. A. Metavitsiadis, X. Zotos, O. S. Barišić, and P. Prelovšek, *Phys. Rev. B* **81**, 205101 (2010).
54. M. Mierzejewski, J. Bonča, and P. Prelovšek, arXiv:1106.0604.
55. for a review see U. Schollwöck, *Rev. Mod. Phys.* **77**, 259 (2005).
56. S. Sota and T. Tohyama, *Phys. Rev. B* **78**, 113101 (2008).
57. J. Kokalj and P. Prelovšek, *Phys. Rev. B* **80**, 205117 (2009).
58. J. Kokalj and P. Prelovšek, *Phys. Rev. B* **82**, 060406(R) (2010).
59. W. F. Brinkman and T. M. Rice, *Phys. Rev. B* **2**, 1324 (1970).
60. J. E. Hirsch, *Phys. Rev. Lett.* **59**, 228 (1987); S. A. Trugman, *Phys. Rev. B* **37**, 1597 (1988); B. I. Shraiman and E. D. Siggia, *Phys. Rev. Lett.* **60**, 740 (1988).
61. P. Prelovšek and X. Zotos, *Phys. Rev. B* **47**, 5984 (1993).
62. J. Riera and E. Dagotto, *Phys. Rev. B* **47**, 15346 (1993); J. Riera and E. Dagotto, *Phys. Rev. B* **57**, 8609 (1998).
63. J. Bonča, S. Maekawa, and T. Tohyama, *Phys. Rev. B* **76**, 035121 (2007).
64. J. Bonča, S. Maekawa, T. Tohyama, and P. Prelovšek, *Phys. Rev. B* **77**, 054519 (2008).
65. L. Vidmar, J. Bonča, and S. Maekawa, *Phys. Rev. B* **79**, 125120 (2009).
66. L. Vidmar, J. Bonča, S. Maekawa, and T. Tohyama, *Phys. Rev. Lett.* **103**, 186401 (2009).
67. L. Vidmar and J. Bonča, *Phys. Rev. B* **82**, 125121 (2010).
68. P. W. Leung, *Phys. Rev. B* **65**, 205101(2002); A. L. Chernyshev, P. W. Leung, and R. J. Gooding, *Phys. Rev. B* **58**, 13594 (1998).
69. P. Wróbel and R. Eder, *Phys. Rev. B* **58**, 15160 (1998).
70. T. J. Park and J. C. Light, *J. Chem. Phys.* **85**, 5870 (1986).
71. N. Mohankumar and S. M. Auerbach, *Comp. Phys. Comm.* **175**, 473 (2006).
72. M. Mierzejewski and P. Prelovšek, *Phys. Rev. Lett.* **105**, 186405 (2010).
73. M. Mierzejewski, L. Vidmar, J. Bonča, and P. Prelovšek, *Phys. Rev. Lett.* **106**, 196401 (2011);
74. L. Vidmar, J. Bonča, M. Mierzejewski, P. Prelovšek, and S. A. Trugman, *Phys. Rev. B* **83**, 134301 (2011).
75. L. Vidmar, J. Bonča, T. Tohyama, and S. Maekawa, arXiv:1107.1040.